27/6/2022

Recycling of calcined carbonated cement pastes as cementitious materials: Proposed CCUS technology for calcium looping

Y.K. Kong [a,b], S.Ruan [b], Kiyofumi Kurumisawa [c*]

[a] Division of Sustainable Resources Engineering, Graduate School of Engineering, Hokkaido University, Japan

[b] College of Civil Engineering and Architecture, Zhejiang University, Hangzhou 310058, China

[c] Division of Sustainable Resources Engineering, Faculty of Engineering, Hokkaido University, Japan

Abstract: In this study, calcined carbonated hydrated cement pastes (HCPs) were used to partially replace ordinary Portland cement (OPC) as a cementitious material. Calcined HCP can be derived from carbonated HCP after the release of CO_2 for the carbon capture, utilization, and storage (CCUS). Calcined carbonated HCP was produced by calcining carbonated HCP at 1000 °C, also used in calcium looping. The crystal phase compositions of the HCP, carbonated HCP, and calcined carbonated HCP were identified. Various hardening and microstructural tests on the composite cement paste mixtures blended with calcined carbonated HCP were performed. The initial results showed that the HCP could sequester CO_2, forming various calcium carbonates.

*Kiyofumi Kurumisawa (kurumi@eng.hokudai.ac.jp, corresponding author); Y.K. Kong (ykkong@elms.hokudai.ac.jp); S. Ruan (sruan001@zju.edu.cn).

After carbonated HCP calcination, the main nanocrystalline phases of calcium silicate hydrate (C-S-H) and calcium carbonate decomposed, forming lime and wollastonite. The 28-day compressive strength of the calcined carbonated HCP−OPC mixtures increased with the replacement ratio up to 20%, owing to the filler effect of wollastonite. The microstructural analysis revealed that the portlandite, C-S-H, and monocarboaluminate phases were formed after hydration. Finally, by recycling demolition waste, this study proposed a technology roadmap for CCUS to achieve this goal, and a life cycle assessment was conducted to evaluate and compare the environmental impacts of producing 1 t of calcined carbonated HCP−OPC mixtures and plain OPC paste.

Keywords: Carbon capture, utilization, and storage; Calcium looping; Calcined carbonated cement paste; Compressive strength; Microstructural analysis; Life cycle assessment.

1. Introduction

Continuous greenhouse gas emissions from human activities have been one of the most severe environmental problems for decades [1]. Greenhouse gases are mainly emitted by industries, of which cement production generates a large volume of CO_2 emissions. [1]. The industrial sector that manufactures ordinary Portland cement (OPC) generates approximately 5%−9% of the total CO_2 anthropogenic emissions [2] [3]. If greenhouse gas emissions are not controlled or mitigated, product proliferation will pose a significant threat to the ecosystem [4].

The two main methods used to reduce CO_2 emissions during concrete production are (1) decreasing the amount of cement produced and (2) capturing the emitted CO_2 within the life cycle of concrete structures [5] [6]. Conventionally, supplementary cementitious materials (SCMs) such as fly ash and granulated ground blast-furnace slag are utilized to partially or wholly replace OPC in concrete [7] [8]. Although SCMs are faced with reaching global limits, the demand for OPC is continuously increasing [5]. Another approach to decreasing the total CO_2 emissions of concrete structures is through carbon capture, utilization, and storage (CCUS), characterized by sustainability and energy savings [9]. CCUS is the process of reducing the CO_2 volume and achieving benefits by converting CO_2 into high-value products for different industries [9] [10]. In the past, CO_2 was sequestered in silica-rich natural rocks [6]. However, the demand for silicate rocks is very high, owing to the large volume of emitted CO_2 [11]. It is estimated that to sequester 1 t of CO_2, approximately 1.6−3.7 t of carbonatable materials are

required, depending on the CO_2 uptake capacity of the materials used [6]. In addition, the associated mining activities and transportation of natural rocks for carbonation can cause significant environmental impacts. To address these limitations, researchers have focused on using demolished concrete structures to replace natural rocks [12] [13].

The use of demolished concrete, characterized by its high alkalinity and abundant Ca^{2+} content, to capture CO_2 has become prevalent in recent years [14] [9]. Unlike the limited natural rock resources, an estimated 900 Mt of demolished concrete is generated annually in Europe, the U.S., and Japan [15]. The components of demolished concrete include aggregates and fully hydrated cement paste (HCP), which is rich in portlandite ($Ca(OH)_2$) and can sequester CO_2 [16] [17]. For demolished concrete, portlandite in HCP should be carbonated. However, because of the initially formed calcium carbonate at the surface of the concrete structure, further carbonation can be prevented by these carbonate products, indicating that the inner portlandite is still not consumed [18] [19]. The carbonation of HCP commences with the penetration of CO_2 into the cement matrix, which dissolves in the pore solution to form CO_3^{2-} ions [12]. These two ions react with portlandite and calcium silicate hydrate (C-S-H), forming various calcium carbonates, such as calcite, vaterite, aragonite, silica gel, and hydrated iron oxides [20] [21]. Adopting HCP from construction waste to capture CO_2 can recycle demolished concrete and produce carbonated cement paste with a significant value. Some researchers have revealed the pozzolanic reactivity of carbonated HCP powders, reporting that they can be utilized as SCMs to partially replace OPC in concrete mixtures [22]. However, the

78 properties of carbonated HCP after CO_2 release through calcination have not been
79 investigated in detail.

80 Numerous studies on using recycled concrete to sequestrate CO_2 have been
81 conducted; most studies focused on the CO_2 capture efficiency of HCP, phase
82 assemblage of HCP after carbonation, and cementitious properties of HCP carbonation
83 [23] [24] [19]. However, a significant aspect of CCUS is the release and reuse of stored
84 (almost pure) CO_2 to manufacture valuable bioproducts [9] [10], which has been
85 neglected by researchers in civil engineering. As mentioned above, the main phase of
86 sequestered CO_2 in HCP carbonation is calcium carbonate ($CaCO_3$). Currently, the
87 conventional method for decomposing $CaCO_3$ is calcination [25]. This approach has
88 been introduced in the thermochemical energy storage system, which relies on the
89 carbonation−calcination reaction of $CaCO_3$/CaO, known as calcium looping (CaL) [26]
90 [27]. For CaL, calcium carbonates are typically derived from natural resources, such as
91 natural limestone and dolomite. Combining CCUS technology with construction and
92 demolition waste to capture CO_2 to generate $CaCO_3$ is more sustainable than collecting
93 natural limestone [27]. Moreover, the traditional CaL requires somewhat high
94 temperatures to convert CaO into $CaCO_3$. The calcination of $CaCO_3$ may still be energy-
95 consuming for $CaCO_3$ decomposition to release CO_2, requiring a temperature range of
96 919−1199 °C (1193−1473 K). Under H_2O steaming conditions, the decomposition
97 temperature can be decreased to 899 °C (1173 K) compared to the direct calcination by
98 combusting fossil fuels [28]. The calcination of carbonated HCP decomposes various

calcium carbonates and the remaining noncarbonated C-S-H when the temperature reaches 700−900 °C, as expressed by Equations (1) and (2) [29].

$$CaCO_3 \rightarrow CaO + CO_2 \uparrow \text{ (Calcination)} \quad (1)$$

$$C\text{-}S\text{-}H \rightarrow CaO + SiO_2 + H_2O \uparrow \text{ (Calcination)} \quad (2)$$

Calcium oxide (CaO) and silica (SiO_2) are cementitious components produced after the calcination of carbonated HCP. CaO is the major chemical oxide in lime that improves the early-age strength of concrete [30], and SiO_2 is highly rich in silica fume, which exhibits strong pozzolanic reactivity and can refine the pore structure of hardened pastes [31]. Lime and silica fume are extensively utilized in construction [30] [32] [33]. Barbhuiya et al. [34] reported that the early-age compressive strength of fly-ash-based concrete could be improved by adding hydrated lime and silica fume. Das et al. [30] observed that fly-ash-based geopolymer concrete attained the highest compressive strength when 7.5% and 2.0% fly ash were replaced with lime and silica fume, respectively. Calcination of carbonated HCP may be the best approach to releasing and utilizing captured CO_2. In a previous study, the authors developed a CO_2 sponge through HCP calcination to recapture CO_2 under saturation conditions. A technology roadmap for recycling HCP, carbonated HCP, and calcined HCP in CCUS was plotted, as reported in Ref. [35]. Therefore, in the previous study, the authors achieved CaL by recycling HCP from demolition waste to repeatedly sequester and release CO_2. In this study, the cementitious potential of calcined carbonated HCP was investigated to extend

and complete the entire recycling cycle of CCUS using HCP. If the cementing effects of calcined carbonated HCP are revealed, CaL products will not be limited to the form of storage media for CO_2.

Therefore, the extensive use of calcined carbonated HCP is proposed, and a novel approach for CCUS can be developed. Previous studies mainly focused on the seeding effect and SCM-like properties of carbonated HCP powders during the hydration of OPC-based mixtures containing carbonated HCP powders [36]. Moreover, the disposal of by-products generated from CO_2-released carbonated HCP has not been investigated extensively. In this study, calcined carbonated HCP was systematically investigated, in which HCP underwent carbonation and calcination. The cementing effects of the calcined carbonated HCP were evaluated through macro- and micro-structural evaluations. Moreover, a life cycle assessment for evaluating environmental impacts during the production of calcined carbonated HCP−OPC mixtures was conducted. It is believed that this study will facilitate the development of CCUS for practical applications.

2. Experimental program

2.1. Materials and preparation of specimens

2.1.1. Preparation of HCP, carbonated HCP, and calcined carbonated HCP

Before preparing carbonated HCP, HCP was manufactured using Type CEM I OPC with a strength class of 42.5 N, complying with ASTM C150 [37]. In actual construction

143 work, HCP can be obtained from demolished concrete using comminution and magnetic
144 methods, which are advanced techniques for producing recycled aggregate concrete [38]
145 [39]. HCP specimens were cast in 100 mm × 100 mm × 100 mm molds with a constant
146 water-to-cementitious material (W/CM) ratio of 0.5, according to ASTM C305
147 requirements [40]. The hardened specimens were cured at 23±0.5 °C and relative
148 humidity of 100%. After curing for one day, the HCP samples were demolded and
149 hydrated at 60±0.5 °C for 90 days, accelerating hydration to simulate the OPC paste
150 derived from demolition waste, consistent with Skocek et al. [6]. The hydration degree
151 of the clinker was close to 90% (not 100%) under the above curing conditions.
152 Moreover, a curing temperature of 60±0.5 °C would not significantly change the
153 microstructure of the cement paste but could accelerate the hydration process [41]. The
154 HCP specimens were then pulverized into 75 μm powders by ball milling and
155 carbonated for 24 h to produce carbonated HCP; the carbonation was conducted in an
156 autoclave, providing a pure CO_2 environment (99.9%) with a constant gas pressure of
157 1.5 MPa. Most recent studies on CaL have been focused on carbonation under low CO_2
158 partial pressure, indicating that low CO_2 concentrations in the flue gas in the power
159 plant were used. However, for thermochemical energy storage in the CaL to sequester
160 CO_2, a high CO_2 concentration (pure CO_2 environment) is required [26]. The
161 carbonation autoclave set can be found in Refs. [35] [42]. The weight differences before
162 and after carbonation were measured. After each carbonated HCP specimen cooled
163 down to room temperature, it was calcined in a muffle furnace to produce calcined
164 carbonated HCP. The initial temperature was 30 °C, which was increased to 1000 °C at

165 a constant heating rate of 4 °C/min. The final temperature (1000 °C) was maintained
166 for 2 h to completely decompose calcium carbonate. This calcination temperature range
167 was consistent with our previous study, and the decomposition products of calcium
168 carbonates were obtained [35]. After calcination, the calcined carbonated HCP was
169 removed and weighed.
170
171 2.1.2. Preparation of composite cement paste
172 Composite cement pastes were prepared using Type CEM I with a strength class of
173 42.5 N, OPC-calcined carbonated HCP, and tap water. The chemical compositions of
174 OPC were determined using X-ray fluorescence spectrometry (XRF), as listed in Table
175 1. Four groups of paste mixtures were produced and subjected to tests to evaluate the
176 influence of HCP calcination on the properties of the OPC pastes. Specifically, they
177 comprised three groups of OPC pastes partially replaced with calcined carbonated HCP
178 (calcined carbonated HCP−OPC pastes) and one group of plain OPC pastes as the
179 reference (Ref.). For consistency, the W/CM ratio was maintained at 0.40 for all the
180 mixtures. The mixing proportions are listed in Table 2. For clarity, each experimental
181 group was labelled "MN," where N denotes the replacement ratio of calcined
182 carbonated HCP in the binder, ranging from 10% to 30%.
183 A Hobart mixer was used to produce paste mixtures according to ASTM C305, and
184 the mixtures were cast in 20 mm × 20 mm × 20 mm molds. Immediately after casting,
185 the fresh paste mixtures were placed on a vibration table and compacted until no visible
186 bubbles appeared on the surfaces of the samples. Next, the samples were covered by a

187 thin cling film and cured at 23±0.5 °C for 24 h. After curing for one day, the samples
188 were demolded and immersed in a water tank at 23±0.5 °C to prevent drying shrinkage.
189
190 2.2. Test methods
191 2.2.1. Compressive strength
192 A hydraulic compression machine was used to determine the 28-day compressive
193 strength of the specimens according to ASTM C109 [43]. The test results for each
194 mixture were calculated as the average strength of triplicate specimens.
195
196 2.2.2. X-ray diffraction (XRD)
197 XRD was conducted to investigate the phase formations of the paste samples.
198 Before the XRD test, the paste samples were crushed and oven-dried for one day.
199 Subsequently, the crushed samples were milled to fine powders (≤ 75 μm) before the
200 XRD tests. XRD patterns were analyzed using an XRD Bruker D8 Advance instrument.
201 The Cu$K\alpha$ X-ray (λ = 1.5418 Å) was generated at 40 mA and 40 kV. Scanning
202 measurements were conducted within a 2θ range from 5° to 90° in a step size of 0.02°.
203
204 2.2.3. Thermogravimetric analysis (TGA)
205 For parallel comparison, milled fine-sized powders of approximately 5.0 mg were
206 used to conduct TGA using a Mettler Toledo STARe System TGA2. The powders were
207 heated from 30 °C up to 1000 °C in open vessels in an N_2 atmosphere at a heating rate

of 15 °C/min. The thermogravimetric (TG) and derivative thermogravimetric (DTG) curves of the paste samples were plotted.

2.2.4. Fourier-transform infrared spectroscopy (FTIR)

A Nicolet iS50 FTIR spectrometer with a frequency range of 4000−400 cm^{-1} at a 4 cm^{-1} resolution was used to obtain the FTIR data of the specimens. Thirty-two scans were recorded for each sample. KBr discs were prepared by pressing pellets composed of the samples and KBr at a ratio of 1:100.

3. Results and discussion

3.1. Before mixing

3.1.1. Weight variations in HCP after carbonation and calcination

Table 3 lists the content for each processing procedure and the weight change ratio after each processing step. A weight increase in HCP was observed after carbonation with an increase ratio of 21.25% because CO_2 was sequestered. A decrease in weight was observed when the carbonated HCP was calcined at 1000 °C. This weight decrease could be attributed to the decomposition of specific phases within the carbonated HCP, and the phases should contain various types of calcium carbonates. The weight decrease ratio of 35.35% was higher than the above weight increase ratio, indicating that other phases other than calcium carbonates decomposed, as discussed later.

3.1.2. XRD patterns

Fig. 1 shows the XRD patterns of the HCP, carbonated HCP, and calcined carbonated HCP. Various hydration products, that is, portlandite (2θ = 18.0°, 34.2°, 47.1°, 54.4°, and 62.6°), C-S-H (2θ = 26.5° and 29.3°), and monocarboaluminate phases, $C_4A\bar{C}H_{11}$ (2θ = 11.6°), were observed in the HCP [22] [44] [45]. In addition, a slight peak was detected at 2θ = 39.3 °, which was attributed to calcite formed by natural carbonation. The presence of calcite leads to the formation of monocarboaluminate [46]. Compared to the HCP, a significant decrease in the intensity of portlandite was detected in the carbonated HCP. In contrast, a conspicuous appearance of calcium carbonate was observed at 2θ = 23.0°, 29.4°,32.5°, 39.3°, 43.2°, 45.9°, and 48.5°, indicating that HCP carbonation consumed the most portlandite, forming various calcium carbonates [47]. The C-S-H did not appear to be significantly carbonated during HCP carbonation, which might be attributed to the preformed calcite layer preventing further C-S-H carbonation [48] [49]. Regarding the calcined carbonated HCP, the crystal phases of calcium carbonates and nanocrystalline phases of C-S-H mentioned above almost vanished [50], whereas CaO was detected (2θ = 37.3°), corresponding to the C-S-H decomposition expressed by Equation (2). Moreover, wollastonite ($CaSiO_3$) was detected at peaks of 23.1°, 32.0°, 41.2°, and 44.8° and a continuous zig-zag pattern of 55°−60° [51] [52] [53]. As expressed by Equations (1) and (2), calcination decomposes calcium carbonates and C-S-H, releasing CO_2 and evaporated H_2O [51]. Calcination could also release pore solutions and gel water, which explains why the weight decrease ratio after calcination exceeded the weight increase ratio after carbonation. Furthermore,

252 the lime and quartz could react in the muffle forming wollastonite at high temperatures
253 up to 1000 °C, owing to the decomposition of C-S-H and calcite, as expressed by
254 Equation (3) [54].
255
256 $CaO + SiO_2 \rightarrow CaSiO_3$ (Calcination) (3)
257
258 3.1.3. TG-DTG curves
259 Fig. 2 shows the TGA results for the HCP, carbonated HCP, and calcined
260 carbonated HCP, consistent with the XRD results. The DTG curves for the three
261 different samples varied significantly, suggesting the formation of different products in
262 the HCP after carbonation and calcination. When the temperature increased from 30 to
263 150 °C, the nanocrystalline phases of C-S-H in the HCP and carbonated HCP
264 dehydrated, indicating that C-S-H essentially remained noncarbonated [13]. However,
265 no weight decrease was observed in the calcined carbonated HCP, possibly owing to
266 hydrated product decomposition caused by calcination. As the temperature increased to
267 400–450 °C, a significant weight decrease was detected in the HCP, attributed to
268 portlandite decomposition [55]; in contrast, the carbonated HCP underwent a slight
269 weight decrease, suggesting that a small portion of the portlandite was noncarbonated.
270 A low and broad maximum appeared on the DTG curve of the calcined carbonated HCP
271 at approximately 400 °C, which should correspond to portlandite decomposition in
272 agreement with the XRD patterns [56]. When heating temperature continued increasing
273 to 800 °C, a broad and high peak occurred in the carbonated HCP because of the

decarbonation of the calcium carbonates. However, a broad and short peak appeared in the HCP curve, attributed to the weak natural carbonation of HCP within its long curing period [49]. Based on the TG results, the CO_2 uptake ratio was calculated using the weight loss difference of the carbonated HCP and calcined carbonated HCP at 500−900 °C, which was 21.61%. This value is close to the weight increase ratio of the HCP after carbonation, indicating that weight gain is generally associated with CO_2 sequestration. It was difficult to observe the weight variation in the calcined carbonated HCP at high temperatures (above 900 °C), demonstrating that CO_2 was entirely released during calcination.

3.2. After producing composite cement paste

3.2.1. Compressive strength

The 28-day compressive strength results for each paste mixture were determined (Fig. 3) to evaluate the influence of HCP calcination on the mechanical properties of the OPC pastes. Overall, the compressive strength first increased with increasing replacement ratio and then decreased. The reference group specimen exhibited a 28-day compressive strength of 37.8 MPa. The compressive strength values of M10 and M20 were higher than that of the reference group, but the compressive strength of M30 decreased significantly. Thus, the strength of the paste mixture increased when the calcined carbonated HCP replacement ratio increased from 0% to 20%, beyond which the strength development of the paste was significantly hindered. Therefore, an optimum calcined carbonated HCP replacement ratio of 20% improved the compressive

strength by up to 8%. The strength improvement caused by HCP calcination might be attributed to the effect of wollastonite. Previous studies have investigated the possibility of mixing ground wollastonite powder in cement pastes and revealed the cementitious properties of wollastonite [52]. Wahab et al. [57] found that using wollastonite to replace 20% sand could improve the mechanical properties of mortar mixtures. Kalla et al. [58] observed that when 10%−15% of cement was replaced with wollastonite, the permeability and chloride diffusion coefficients of concrete mixtures decreased. Both studies reported an optimum ratio of 20% for using wollastonite to replace other construction materials, consistent with the compressive strength results. The beneficial effect of wollastonite on hydration behavior can be attributed to the filler effect and reduced heat generation [53] [52]. The surface areas of finer wollastonite provide additional nucleation sites for C-S-H growth [59]. However, with a slight increase in the replacement ratio, the dilution effect caused by the calcined carbonated HCP may decrease the strength of the paste mixtures [60]. Hence, it is possible to utilize calcined carbonated HCP to partially replace cement at the optimum content, maintaining the same or improved mechanical properties.

3.2.2. XRD

Fig. 4 shows the XRD patterns of the paste mixtures after curing for 28 days. Common hydration products, including portlandite, C-S-H, and monocarboaluminate, were detected in all the groups. A low and narrow peak at $2\theta = 39.3°$ was observed, related to atmospheric carbonation during curing and measurements. No significant

differences between the M10, M20, and reference groups were observed. However, a sharp peak with a significantly high portlandite intensity (2θ = 18.0°) was observed in M30, owing to the high replacement ratio of calcined carbonated HCP containing a comparatively larger amount of CaO, which reacted with H_2O to form portlandite. Moreover, the C-S-H intensity at 2θ = 29.3° was lower than that of the reference group, probably because the higher calcined carbonated HCP content diluted the clinker [60]. The XRD results are consistent with the compressive strength results. The calcined carbonated HCP increased the strength, although the degree of improvement was insignificant. Moreover, the XRD patterns of the Ref., M10, and M20 groups were similar. A significant decrease in the compressive strength of M30 was observed from the XRD patterns, with a significantly higher portlandite intensity and lower C-S-H intensity than those of the other groups.

3.2.3. TGA

Fig. 5 shows the DTG and TG curves of the paste mixtures. The TGA results were consistent with the XRD patterns and compressive strength measurements. Three main decomposition steps were observed in the DTG curves in agreement with previous findings [13] [55] [56] [31], identified as follows:

(1) 30−300 °C: Dehydration of water bonded to C-S-H.

(2) 300−500 °C: Decomposition of portlandite.

(3) 500 − 900 °C: Decarbonation of various calcium carbonates, including amorphous calcium carbonates, vaterite, aragonite, and calcite.

The weight loss percentages of the paste mixtures associated with the water and CO_2 contents are listed in Table 4. The carbonation degree, represented by amorphous calcium carbonates (~650 °C), was also reflected. A minimal difference in weight loss was observed for all the paste mixtures, consistent with the similar XRD patterns among the reference and experimental groups. Moreover, the total weight loss of the experimental groups increased with an increase in the calcined carbonated HCP content, attributed to the increased portlandite content. A similar total weight loss of approximately 21% revealed by these mixtures was consistent with the 28-day compressive strength results, indicating a relationship between the extent of hydration and the mechanical properties [13].

3.2.4. FTIR

Fig. 6 shows the FTIR spectra of the OPC pastes containing partially replaced calcined carbonated HCP after curing for 28 days. No significant differences among the four groups of paste mixtures were observed, consistent with the XRD patterns and TG-DTG curves. Six major bands were observed in all the specimens. First, a sharp absorption at 3644 cm^{-1} was detected, associated with the symmetrical stretching vibration of hydroxyl groups [61]. A wide band at a wavenumber of approximately 3500 cm^{-1} revealed the existence of portlandite in the reference and experimental groups [62]. All the specimens showed a narrow absorption band at wavenumbers of 1500−1750 cm^{-1}, corresponding to the water content (for example, gel water) in the cement matrix. Subsequently, a significant band at approximately 1450 cm^{-1} was detected, owing to the

362 v_2 bending vibration of C-O [61]. As mentioned earlier, the existence of C-O was
363 attributed to natural carbonation, in agreement with the TGA results. A broad absorption
364 band was observed at approximately 970 cm^{-1}, associated with the Si-O in-plane
365 stretching vibration of the Q_2 tetrahedra in C-S-H gels [63]. No distinct shifts in the
366 wavenumber of Si-O stretching bands were observed for the reference and experimental
367 groups. This indicates that an increased replacement ratio of calcined carbonated HCP
368 in the binder system would not significantly influence Si polymerization, consistent
369 with the characterization and mechanical test results.
370
371 **4. Further discussion**
372 Consistent with previous findings [22] [16] [64], the ability of HCP to sequester
373 CO_2 leads to the formation of carbonated HCP. After the calcination of carbonated HCP,
374 the crystal phases of portlandite, C-S-H, and calcium carbonates decomposed, and new
375 phases of lime and wollastonite were formed. With dehydration and decarbonation,
376 water and CO_2 were released, generating the discrepancy between the weight increase
377 in HCP after carbonation and the weight decrease in carbonated HCP after calcination.
378 Furthermore, the mechanical properties of the OPC pastes partially replaced with
379 calcined carbonated HCP were consistent with the hydration degree. Facilitated by
380 microscopic investigations, the hydration behaviors of the calcined carbonated HCP−
381 OPC pastes are discussed below.
382
383 4.1. Hydration behaviors of calcined carbonated HCP−OPC paste mixtures

Based on the detailed investigation of Ref., M10, M20, and M30, the hydration mechanism of the calcined carbonated HCP−OPC paste mixtures is evident. Fig. 7 depicts the underlying mechanisms of the hydration behavior. Based on the mechanical and microscopic test results, the cementing effect of calcined carbonated HCP was observed, owing to the presence of lime, silica, and wollastonite, which were formed from the dehydrated C-S-H, portlandite, and decarbonated calcium carbonates. After mixing, the added wollastonite in the calcined carbonated HCP provided nucleation sites for cement hydration, favoring C-S-H growth. In addition, silica reacted with $Ca(OH)_2$-rich pore solutions to generate additional C-S-H, improving the compressive strength [65]. The slight improvement in the 28-day compressive strength might also be influenced by the filling effect of wollastonite, leading to pore densification. Furthermore, the dilution effect of the calcined carbonated HCP should be considered, as wollastonite did not contribute to the strength gain. Because of these two contrasting effects on cement hydration, an optimum replacement ratio (20%) of calcined carbonated HCP existed in the binder system, at which the strength enhancement effect could compensate for the dilution effect. Above this optimum replacement ratio, the dilution effect was the dominant mechanism, and the mechanical properties of the composite cement pastes decreased significantly. Moreover, a higher amount of calcined carbonated HCP produced a higher portlandite content, which might cover the calcium silicate surface and prevent further hydration.

4.2. Proposed CCUS technology routine

406 Regarding the cementing effect of calcined carbonated HCP, recycling carbonated
407 HCPs in CCUS is feasible. Fig. 8 shows a technology roadmap of CCUS using
408 demolished concrete structures. During this process, CO_2 undergoes five stages: 1)
409 emission from the concrete structure, 2) capture by HCP, 3) transportation, 4)
410 calcination for release, and 5) reuse. CCUS starts from the assumed 1 t of CO_2 emitted
411 during the production and demolition of concrete structures. According to the
412 Intergovernmental Panel on Climate Change [66], CO_2 can be generated within the
413 entire life cycle of a concrete structure, from concrete production to the demolition of
414 the structure, as shown by the rectangle plotted by the dashed line in the roadmap. The
415 total amount of HCP used was 1000 kg. The CO_2 flow was quantitatively evaluated in
416 each step, and the CO_2 sequestering and release ratios were based on the experimental
417 results of this study. After demolition, concrete waste can be sorted into aggregates and
418 HCP. The aggregates can be used as recycled aggregates for producing new concrete,
419 and the HCP can be used as the sequestering media for the emitted CO_2 during the
420 service life of the concrete structure. A total of 210 kg of CO_2 was captured in the HCP
421 as the formed calcium carbonates in the first recycling phase and transported (for
422 example, using a lorry) without pipeline networks, significantly decreasing the energy
423 penalty [11]. Carbonated HCP can be calcined to release CO_2, which can be further
424 dried, purified, and stored to manufacture valuable industrial products, such as biofuels
425 and plastic [67]. The 786 kg calcined carbonated HCP produced during the CO_2 release
426 stage can be used as a cementitious material in concrete, as mentioned previously. With
427 such a technology roadmap, 210 kg of CO_2 can be captured and utilized from concrete

demolition wastes, and 786 kg of valuable calcined carbonated HCP can be collected for concrete production in a recycling phase, which is somewhat efficient and ecofriendly.

4.3. Life cycle assessment (LCA) for producing 1 t calcined carbonated HCP–OPC mixtures

A typical "cradle-to-grave" LCA was conducted according to the International Organization for Standards 14040 (ISO 14040) [68]. In this study, the CML 2002 approach, one of the most widely used methodologies, was used to evaluate and compare the environmental impacts of producing 1 ton of M20 and OPC pastes [68].

4.3.1. Goal, scope, and system boundary

The system boundary covers raw material production to the final product packing [69]. Two materials, that is, plain OPC paste and calcined carbonated HCP–OPC paste, were adopted to compare their environmental impacts. M20 (80 wt.% OPC and 20 wt.% calcined carbonated HCP with a W/CM ratio of 0.4) and OPC paste (100 wt.% OPC with a W/CM ratio of 0.4) were selected. M20 was chosen for the LCA because it exhibited the best strength performance among the three mixtures with different replacement ratios. The functional unit of the LCA was 1 t of M20 and OPC pastes under the same curing conditions (Table 5). The process flow diagrams for the M20 and OPC pastes are shown in Fig. 9, where the dashed lines represent the system boundaries for both materials. Before analysis, some assumptions were made. 1) The transportation

and use phases might have environmental impacts, although these two phases were assumed to be the same with the various types of concrete. 2) All OPC pastes used to produce the M20 and OPC pastes were obtained from Europe for consistency. 3) Because the demolished concrete could be derived entirely from the waste, the environmental impacts caused by recycling demolished concrete were neglected in this LCA; however, the CCUS technology for manufacturing calcined carbonated HCP should be considered. The CCUS technology process can be considered a roadmap (Fig. 8).

4.3.2. Inventory

For the LCA, inventory data for the raw materials and processing procedures were acquired from the Ecoinvent database and existing literature [70] [71] [72] [73] [74] [75]. The details of the raw materials used for manufacturing the M20 and OPC pastes are described below.

The OPC produced from the clinker and gypsum was set as CEM I 42.5 N-type cement. Boesch and Hellweg reported life-cycle impact assessment (LCIA) results for cement production in Europe [76]. Hence, the detailed OPC production processes, including crushing, milling, blending, and calcination, are not described in this paper [73]. The environmental impact data for tap water were collected directly from the Ecoinvent database. The production of calcined carbonated HCP powder is complicated because of its CCUS process, which consists of crushing and screening HCP from demolished waste, sequestering CO_2 in HCP, and calcining carbonated HCP. The

environmental impacts of the crushing and milling phases are explained in *Table of Bond Work Index by Minerals*[1]. Mercante et al. [75] reported the energy and material input for sorting and recycling mixed construction and demolition waste (concrete), in which diesel fuel, electrical energy, and water accounted for 1.02 L, 2.59 kWh, and 1.00 L, respectively, for 1 t waste. Owing to the limited research on recycling HCP from demolition waste, the life cycle inventory of HCP collection was performed for the recycled aggregate production, as reported in [77] [78] [79] [80]. HCP carbonation requires gas pressure. As mentioned above, CO_2 gas pressure of 1.5 MPa was applied for carbonation. Therefore, the LCIA data for carbonation were used as compressed air with an average generation of <30 kW 12 bar gauge according to the Ecoinvent database. The required CO_2 volume for HCP carbonation to produce 143 kg of calcined carbonated HCP was calculated based on the experimentally used autoclave. Based on the experimental results for the weight change ratio and TGA for the HCP, carbonated HCP, and calcined carbonated HCP, 220 kg of carbonated HCP and 174 kg of HCP were required. Typically, HCP accounts for 25 wt.% in concrete; therefore, the estimated total weight of demolished concrete was 696 kg [81]. Considering the time required for carbonation to reach equilibrium (the gas pressure inside the chamber does not change with time), the required CO_2 volume for HCP carbonation was 3.08 m^3. Finally, the calcination of carbonated HCP (also called CO_2 separation) was conducted at 1000 °C, but the actual decomposition temperature of $CaCO_3$ generally ranged from 500 to

[1] Table of Bond Work Index by Minerals: https://www.911metallurgist.com/blog/table-of-bond-work-index-by-minerals

900 °C, as measured using TGA. Therefore, it was assumed that the starting temperature was room temperature, and $CaCO_3$ decomposition was completed at 900 °C. The calcination process for converting calcium carbonates into CaO is the most energy-intensive stage [82]. Giordano et al. [83] reported in detail the LCA of postcombustion CO_2 capture, in which the LCIA of CO_2 separation related to natural gas combustion in an auxiliary gas turbine (functional unit of per ton CO_2) was used to calculate the environmental impacts of the calcination phase of the proposed CCUS roadmap. Based on the above discussion, the LCIA of the CCUS technology in the proposed roadmap is presented in Table 6.

4.3.3. Impact assessment of M20 and OPC paste production

Five baseline categories were adopted to estimate the environmental impacts of producing M20 and OPC pastes. These categories are global warming potential (GWP), ozone depletion potential (ODP), photochemical ozone creation potential (POCP), acidification potential (AP), and eutrophication potential (EP) [84]. The functional units of GWP, ODP, POCP, AP, and EP are kg CO_2-eq., kg CFC-11-eq., kg C_2H_4-eq., kg SO_2-eq., and kg PO_4^{3-}-eq., respectively.

Based on this classification, the impact assessment of the raw materials used for producing M20 and plain OPC paste and the total environmental impact were determined (Table 7). Cement production in manufacturing 1 t of M20 and OPC paste was dominant in GWP, ODP, POCP, AP, and EP. For the OPC paste, water production generally had no significant impact in these five categories, and the highest degree of

514 the environmental impact of water production was 1.21% for ODP. For M20, calcined
515 carbonated HCP production may result in high greenhouse gas emissions. However,
516 because of the lower amount of calcined carbonated HCP in M20, the environmental
517 impact of HCP calcination (3.63%) was significantly lower than that of cement
518 production (96.35%) in GWP. The most significant effect of the calcined carbonated
519 HCP was observed for the ODP, which accounted for 16.35% of the total impact. The
520 difference ratios of LCIA for the GWP, ODP, POCP, AP, and EP between these two
521 materials were calculated as ($LCIA_{M20} - LCIA_{OPC\ paste}$)/$LCIA_{OPC\ paste}$ (Table 7) to
522 compare the environmental impacts of M20 and OPC pastes. The results showed that
523 the total environmental impacts of producing 1 t of M20 were less severe than those of
524 OPC paste, particularly for EP, which decreased by up to 17.7%. Thus, calcined
525 carbonated HCPs satisfy the required mechanical properties of construction materials
526 and are ecofriendlier than conventional cement-based materials.
527
528 4.4. Limitations of CCUS technology
529 Although the CO_2 transport routine from the emission source to the reuse in
530 bioproduct manufacture was qualitatively and quantitatively clarified in the proposed
531 technology route. Calcination of carbonated HCP for releasing captured CO_2 is still not
532 an ideal method because of the non-negligible energy consumption. In future studies,
533 the release of CO_2 from carbonated HCP without calcination should be further
534 investigated. If solved, the CaL technique can also be improved. However, CCUS
535 technology still faces various penalties and limitations, such as energy consumption,

financial needs, and public awareness. [85] [86]. Leonzio et al. [85] reported a net present value of 0.554 trillion euros and a payback period of 2.85 years for the best CCUS supply chain. Saito et al. [87] conducted a survey to assess the current status of general public awareness and opinion on CCUS in Japan. They observed a somewhat low level of climate change consciousness and a passive attitude toward CCUS policies. Moreover, two cases of CO_2 storage are discussed, demonstrating the restrictions of CCUS in many countries. The CO_2-EOR project in Gao 89 is a CO_2 geological storage project in China. CO_2 injection and storage were analyzed by Ma et al. [88]. Four CO_2 gas wells, that is, Gao 89-4, Gao 89-5, Gao 89-16, and Gao 89-17, were selected to calculate the accumulated amount of CO_2 injected and generated. A total of 62,000 tons of CO_2 was injected, and a total of 58634.71 tons of CO_2 was stored underground by the end of 2011. During this process, investment in the project cannot be ignored. Such techniques for reducing and storing anthropogenic CO_2 are limited and significantly less effective than expected. Another example is the multicriteria analysis conducted by Vögele et al., which evaluated the feasibility of CCUS in Germany [11]. They compared the possible impacts of deploying CCUS in six scenarios (REF, REF_high, CCS, CCS_high, REG, and REG_high), which differed in renewables and certificate prices. The results indicate a gloomy future for the CCUS technology in Germany. Because of the overall cost of the electricity supply system and the cost sensitivity to changes in the CO_2 allowance, several disadvantages exist in the operation phase of the electricity supply equipped with CCUS technology. The uncertainties in the feasibility of this technique account for a higher risk, hindering CCUS development. Governmental

regulations regarding CCUS may raise companies' unwillingness to apply CCUS. Hence, simultaneously achieving economy, energy conservation, and public acceptance is still a considerable task for researchers and workers in CCUS.

5. Conclusions

In this study, the phase compositions of calcined carbonated HCP and the effect of calcined carbonated HCP powders on the performance of OPC-based pastes were investigated. Calcined carbonated HCP was manufactured using HCPs subjected to carbonation and calcination. Various tests, including the compressive strength test, XRD, TGA, and FTIR, were performed. An LCA was then conducted to evaluate and compare the environmental impacts of producing 1 t of M20 and OPC pastes. The following conclusions were drawn.

(1) Based on the TGA results, HCP carbonation significantly consumed portlandite to form calcium carbonates, with a CO_2 uptake ratio of 21.61%. C-S-H in the HCP generally remained noncarbonated, which may be attributed to the newly formed calcite, preventing further gaseous CO_2 penetration.

(2) The calcination of carbonated HCP decomposed the main nanocrystal phase of C-S-H and the crystal phases of portlandite and various calcium carbonates, forming lime and wollastonite.

(3) At the same W/CM ratio of 0.4, the partial replacement of calcined carbonated HCP increased the 28-day compressive strength by up to 8%, with an optimum

580 replacement ratio of 20%. This was because of the filler effect of wollastonite and the
581 early-age strength improvement effect of lime; above the optimum replacement ratio,
582 the strength significantly decreased because of the dilution effect.
583 (4) Based on the microscopic characterizations, the major crystal phases in calcined
584 carbonated HCP − OPC pastes were identified, including C-S-H, portlandite,
585 monocarboaluminate, and some calcium carbonates formed by natural carbonation. The
586 crystal phases generally remained unchanged with an increasing replacement ratio of
587 calcined carbonated HCP.
588 (5) Finally, a conceptual technology roadmap for CCUS adopting HCP was
589 proposed. In addition, the LCA impacts of producing 1 t of M20 were less severe than
590 those of plain OPC paste in the five environmental impact categories (GWP, ODP,
591 POCP, AP, and EP). This study provides a reference for applying demolition waste in
592 CCUS and concrete production.

Conflict of interest

The authors declare that there is no conflict of interest.

Data availability statement

Some or all data, models, and codes that support the findings of this study are available from the corresponding author upon reasonable request.

601 **Tables**

602 Table 1. Chemical compositions of OPC by mass (wt.%).

Component	Cement
CaO	63.57
SiO_2	20.58
Al_2O_3	4.97
Fe_2O_3	3.76
SO_3	2.00
MgO	2.29
f-CaO	0.75
Na_2Oeq	0.53
LOI	1.40

603

604 Table 2. Mixing proportions.

Mixture ID	OPC/g	HCP-calcination/g	Water/g	Total weight/g	Replacement ratio/%
Ref.	42.86	0	17.14	60	0
M10	38.57	4.29			10
M20	34.29	8.57			20
M30	30.00	12.86			30

605

606 Table 3. Details of samples at each processing stage.

Sample	Content	Processing procedure	Weight/g *		Weight change ratio/%
			Before	After	
HCP	Fully hydrated cement paste	Hydrated for 3 months at 60 ± 0.5 °C	-	-	-
HCP-carbonation	Carbonated HCP	Carbonation for 24 hours at constant gas pressure of 1.5 MPa and constant temperature of 60 ± 0.5 °C	120.0	145.5	21.25
HCP-calcination	Calcined HCP-carbonation	Calcination at 1000 °C	135.8	87.8	35.35

607 *Weights of samples before and after processing are listed in the fourth and fifth

608 columns, respectively. These abbreviations were also used in the figures.

609

610 Table 4. Quantification of water and CO_2 contents calculated using TGA.

Mix	Weight loss percentage (%)					
	30-300 °C	300-500 °C	500-900 °C	H_2O	CO_2	Total
Ref.	9.02	5.76	6.65	14.78	6.65	21.43
M10	9.31	5.75	6.08	15.06	6.08	21.14
M20	9.37	5.94	5.92	15.31	5.92	21.23
M30	9.71	6.40	6.65	16.11	6.65	22.76

611

612 Table 5. Production of 1 t M20 and OPC paste.

Raw materials	OPC cement/kg	HCP-calcination /kg	Water/kg
M20	572	143	285
OPC paste	715	0	285

613

614 Table 6. Environmental impacts of producing 143 kg calcined HCP.

Procedure	GWP/kg CO_2-eq.	ODP/kg CFC-11-eq.	POCP/kg C_2H_4-eq.	AP/kg SO_2-eq.	EP/kg PO_4^{3-}-eq.
Crushing and screening	8.004	1.559×10^{-6}	2.847×10^{-3}	0.056	3.605×10^{-3}
Carbon capture	0.010	3.883×10^{-13}	4.231×10^{-7}	3.125×10^{-4}	8.690×10^{-9}
Calcination	11.448	9.850×10^{-7}	5.220×10^{-4}	6.490×10^{-3}	1.130×10^{-3}
Total environmental impacts	19.462	2.544×10^{-6}	3.369×10^{-3}	0.0630	4.735×10^{-3}

615

616 Table 7. Environmental impacts of producing 1 t M20 and OPC paste.

Materials	Mixture type	GWP/kg CO_2-eq.	ODP/kg CFC-11-eq.	POCP/kg C_2H_4-eq.	AP/kg SO_2-eq.	EP/kg PO_4^{3-}-eq.
OPC	M20	516.516	1.282×10^{-5}	0.024	1.293	0.168
	OPC paste	645.645	1.602×10^{-5}	0.030	1.616	0.210

Water	M20	0.122	1.967×10^{-7}	2.327×10^{-12}	2.454×10^{-5}	6.505×10^{-9}
	OPC paste	0.122	1.967×10^{-7}	2.327×10^{-12}	2.454×10^{-5}	6.505×10^{-9}
HCP-calcination	M20	19.462	2.544×10^{-6}	3.369×10^{-3}	0.0630	4.735×10^{-3}
	OPC paste	0	0	0	0	0
Total environmental impacts	M20	536.101	1.556×10^{-5}	0.027	1.356	0.173
	OPC paste	645.767	1.622×10^{-5}	0.030	1.616	0.210
Difference ratio (%)		-17.0	-4.1	-8.8	-16.1	-17.7

617

618

References

[1] E. Benhelal, G. Zahedi, E. Shamsaei, A. Bahadori, Global strategies and potentials to curb CO_2 emissions in cement industry, J. Clean. Prod. 51 (2013) 142-161. https://doi.org/10.1016/j.jclepro.2012.10.049.

[2] C. Chen, G. Habert, Y. Bouzidi, A. Jullien, Environmental impact of cement production: Detail of the different processes and cement plant variability evaluation, J. Clean. Prod. 18 (2010) 478-485. https://doi.org/10.1016/j.jclepro.2009.12.014b.

[3] J. Li, L. Spanu, J. Heo, W. Zhang, D.W. Gardner, C. Carraro, R. Maboudian, P.J.M. Monteiro, Sequestration of solid carbon in concrete: A large-scale enabler of lower-carbon intensity hydrogen from natural gas, MRS Bull. 46 (8) (2021) 680-686. https://doi.org/10.1557/s43577-021-00118-z.

[4] X.F. Zhang, S.Y. Zhang, Z.Y. Hu, G. Yu, C.H. Pei, R.N. Sa, Identification of connection units with high ghg emissions for low-carbon product structure design, J. Clean. Prod. 27 (2012) 118-125. https://doi.org/10.1016/j.jclepro.2012.01.011.

[5] K.L. Scrivener, V.M. John, E.M. Gartner, Eco-efficient cements: Potential economically viable solutions for a low- CO_2 cement-based materials industry, Cem. Concr. Res. 114 (2018) 2-26. https://doi.org/10.1016/j.cemconres.2018.03.015.

[6] J. Skocek, M. Zajac, M. Ben Haha, Carbon capture and utilization by mineralization of cement pastes derived from recycled concrete, Sci. Rep. 10 (1) (2020) 5614. https://doi.org/10.1038/s41598-020-62503-z.

[7] C. Ridtirud, C. Prinya, Influences of the ratios of high-calcium fly ash to low-calcium fly ash on the strength and drying shrinkage of geopolymer mortar, Adv. Mater. Res. 931-932 (2014) 416-420. https://doi.org/10.4028/www.scientific.net/AMR.931-932.416.

[8] L.A. Qureshi, B. Ali, A. Ali, Combined effects of supplementary cementitious materials (silica fume, GGBS, fly ash and rice husk ash) and steel fiber on the hardened properties of recycled aggregate concrete, Constr. Build. Mater. 263 (2020) 120636. https://doi.org/10.1016/j.conbuildmat.2020.120636.

[9] F.M. Baena-Moreno, M. Rodríguez-Galán, F. Vega, B. Alonso-Fariñas, L.F. Vilches Arenas, B. Navarrete, Carbon capture and utilization technologies: A literature review and recent advances, Energ. Sources. A 41 (12) (2019) 1403-1433. https://doi.org/10.1080/15567036.2018.1548518.

[10] R. Zevenhoven, J. Fagerlund, J.K. Songok, CO_2 mineral sequestration: Developments toward large-scale application, Greenhouse Gases: Sci. Technol. 1 (1) (2011) 48-57. https://doi.org/10.1002/ghg3.7.

[11] S. Vögele, D. Rübbelke, P. Mayer, W. Kuckshinrichs, Germany's "no" to carbon capture and storage: Just a question of lacking acceptance?, Appl. Energy 214 (2018) 205-218. https://doi.org/10.1016/j.apenergy.2018.01.077.

[12] B. Šavija, M. Luković, Carbonation of cement paste: Understanding, challenges, and opportunities, Constr. Build. Mater. 117 (2016) 285-301. https://doi.org/10.1016/j.conbuildmat.2016.04.138.
[13] S. Ruan, C. Unluer, Influence of mix design on the carbonation, mechanical properties and microstructure of reactive mgo cement-based concrete, Cem. Concr. Compos. 80 (2017) 104-114. https://doi.org/10.1016/j.cemconcomp.2017.03.004.
[14] E.R. Bobicki, Q. Liu, Z. Xu, H. Zeng, Carbon capture and storage using alkaline industrial wastes, Prog. Energy Combust. Sci. 38(2) (2012) 302-320.
[15] N.D. Oikonomou, Recycled concrete aggregates, Cem. Concr. Compos. 27 (2) (2005) 315-318. https://doi.org/10.1016/j.cemconcomp.2004.02.020.
[16] P.H.R. Borges, J.O. Costa, N.B. Milestone, C.J. Lynsdale, R.E. Streatfield, Carbonation of CH and C–S–H in composite cement pastes containing high amounts of BFS, Cem. Concr. Res. 40 (2) (2010) 284-292. https://doi.org/10.1016/j.cemconres.2009.10.020.
[17] L. Wang, J. Wang, X. Qian, P. Chen, Y. Xu, J. Guo, An environmentally friendly method to improve the quality of recycled concrete aggregates, Constr. Build. Mater. 144 (2017) 432-441. https://doi.org/10.1016/j.conbuildmat.2017.03.191.
[18] M. Zajac, J. Skocek, J. Skibsted, M. Ben Haha, CO_2 mineralization of demolished concrete wastes into a supplementary cementitious material – a new CCU approach for the cement industry, RILEM Technical Letters 6 (0) (2021) 53-60. https://doi.org/10.21809/rilemtechlett.2021.141.
[19] M. Zajac, J. Skocek, P. Durdzinski, F. Bullerjahn, J. Skibsted, M. Ben Haha, Effect of carbonated cement paste on composite cement hydration and performance, Cem. Concr. Res. 134 (2020) 106090. https://doi.org/10.1016/j.cemconres.2020.106090.
[20] S. Ortaboy, J. Li, G. Geng, R. Myers, P. Monteiro, R. Maboudian, C. Carraro, Effects of CO_2 and temperature on the structure and chemistry of C–(A–)S–H investigated by Raman spectroscopy, RSC Adv. 7 (2017) 48925-48933. https://doi.org/10.1039/C7RA07266J.
[21] M. Fernández Bertos, S.J.R. Simons, C.D. Hills, P.J. Carey, A review of accelerated carbonation technology in the treatment of cement-based materials and sequestration of CO_2, J. Hazard. Mater. 112 (3) (2004) 193-205. https://doi.org/10.1016/j.jhazmat.2004.04.019.
[22] B. Lu, C. Shi, J. Zhang, J. Wang, Effects of carbonated hardened cement paste powder on hydration and microstructure of portland cement, Constr. Build. Mater. 186 (2018) 699-708. https://doi.org/10.1016/j.conbuildmat.2018.07.159.
[23] L. Liu, Y. Ji, F. Gao, L. Zhang, Z. Zhang, X. Liu, Study on high-efficiency CO_2 absorption by fresh cement paste, Constr. Build. Mater. (2020) 121364. https://doi.org/10.1016/j.conbuildmat.2020.121364.
[24] R. Hay, J. Li, K. Celik, Phase evolution, micromechanical properties, and morphology of calcium (alumino)silicate hydrates C-(A-)S-H under carbonation, Cem. Concr. Res. 152 (2022) 106683. https://doi.org/10.1016/j.cemconres.2021.106683.

[25] Y. Wang, S. Y. Lin, Y. Suzuki., Limestone calcination with CO_2 capture (I), decomposition behavior in a CO_2 atmosphere, Energy Fuels 21 (2007) 3317-3321. https://doi.org/10.1021/ef700318c.
[26] C. Ortiz, J.M. Valverde, R. Chacartegui, L.A. Perez-Maqueda, P. Giménez, The calcium-looping ($CaCO_3$/CaO) process for thermochemical energy storage in concentrating solar power plants, Renew. Sustain. Energy Rev. 113 (2019) 109252. https://doi.org/10.1016/j.rser.2019.109252.
[27] G. Colelli, R. Chacartegui, C. Ortiz, A. Carro, A.P. Arena, V. Verda, Life cycle and environmental assessment of calcium looping (CaL) in solar thermochemical energy storage, Energ. Convers. Manage. 257 (2022) 115428. https://doi.org/10.1016/j.enconman.2022.115428.
[28] S. Lin, T. Kiga, Y. Wang, K. Nakayama, Energy analysis of $CaCO_3$ calcination with CO_2 capture, Energy Procedia 4 (2011) 356-361. https://doi.org/10.1016/j.egypro.2011.01.062.
[29] Z.C. Wang, Q. Bai, G. Dresen, R. Wirth, B. Evans, High-temperature deformation of calcite single crystals, J. Geophys. Res. Solid Earth 101 (B9) (1996) 20377-20390. https://doi.org/10.1029/96jb01186.
[30] S.K. Das, S.M. Mustakim, A. Adesina, J. Mishra, T.S. Alomayri, H.S. Assaedi, C.R. Kaze, Fresh, strength and microstructure properties of geopolymer concrete incorporating lime and silica fume as replacement of fly ash, J. Build. Eng. 32 (2020) 101780. https://doi.org/10.1016/j.jobe.2020.101780.
[31] J. Li, Q. Jin, W. Zhang, C. Li, P.J.M. Monteiro, Microstructure and durability performance of sustainable cementitious composites containing high-volume regenerative biosilica, Resour. Conserv. Recycl. 178 (2022) 106038. https://doi.org/10.1016/j.resconrec.2021.106038.
[32] H. Mehdizadeh, E. Najafi Kani, A. Palomo Sanchez, A. Fernandez-Jimenez, Rheology of activated phosphorus slag with lime and alkaline salts, Cem. Concr. Res. 113 (2018) 121-129. https://doi.org/10.1016/j.cemconres.2018.07.010.
[33] M. Mazloom, A.A. Ramezanianpour, J.J. Brooks, Effect of silica fume on mechanical properties of high-strength concrete, Cem. Concr. Compos. 26 (4) (2004) 347-357. https://doi.org/10.1016/S0958-9465(03)00017-9.
[34] S.A. Barbhuiya, J.K. Gbagbo, M.I. Russell, P.A.M. Basheer, Properties of fly ash concrete modified with hydrated lime and silica fume, Constr. Build. Mater. 23 (10) (2009) 3233-3239. https://doi.org/10.1016/j.conbuildmat.2009.06.001.
[35] Y.K. Kong, Y. Song, K. Kurumisawa, T. Wang, D. Yan, Q. Zeng, X. Zhou, S. Ruan, Use of hydrated cement pastes (HCP) as a CO_2 sponge, J. CO2 Util. 55 (2022) 101804. https://doi.org/10.1016/j.jcou.2021.101804.
[36] C. Unluer, A. Al-Tabbaa, Impact of hydrated magnesium carbonate additives on the carbonation of reactive mgo cements, Cem. Concr. Res. 54 (2013) 87-97. https://doi.org/10.1016/j.cemconres.2013.08.009.
[37] ASTM C150/C150M-20, Standard specification for Portland cement, ASTM International, West Conshohocken, PA (2020).

[38] C. Shi, Y. Li, J. Zhang, W. Li, L. Chong, Z. Xie, Performance enhancement of recycled concrete aggregate – a review, J. Clean. Prod. 112 (2016) 466-472. https://doi.org/10.1016/j.jclepro.2015.08.057.
[39] A. Carriço, J.A. Bogas, S. Hu, S. Real, M.F. Costa Pereira, Novel separation process for obtaining recycled cement and high-quality recycled sand from waste hardened concrete, J. Clean. Prod. 309 (2021) 127375. https://doi.org/10.1016/j.jclepro.2021.127375.
[40] ASTM C305, Standard practice for mechanical mixing of hydraulic cement pastes and mortars of plastic consistency, ASTM International, PA (2020).
[41] B. Lothenbach, T. Matschei, G. Möschner, F. Glasser, Thermodynamic modeling of the effect of temperature on the hydration and porosity of portland cement, Cem. Concr. Res. 38 (2008) 1-18. https://doi.org/10.1016/j.cemconres.2007.08.017.
[42] T. Wang, H. Huang, X. Hu, M. Fang, Z. Luo, R. Guo, Accelerated mineral carbonation curing of cement paste for CO_2 sequestration and enhanced properties of blended calcium silicate, Chemical Engineering Journal 323 (2017) 320-329. https://doi.org/10.1016/j.cej.2017.03.157.
[43] ASTM C109/C109M-20b, Standard test method for compressive strength of hydraulic cement mortars (using 2-in. or [50 mm] cube specimens), ASTM International, West Conshohocken, PA (2020).
[44] H. Ye, L. Huang, Degradation mechanisms of alkali-activated binders in sulfuric acid: The role of calcium and aluminum availability, Constr. Build. Mater. 246 (2020) 118477. https://doi.org/10.1016/j.conbuildmat.2020.118477.
[45] J.L. Provis, A. Palomo, C. Shi, Advances in understanding alkali-activated materials, Cem. Concr. Res. 78 (2015) 110-125. https://doi.org/10.1016/j.cemconres.2015.04.013.
[46] R. Snellings, G. Mertens, J. Elsen, Supplementary cementitious materials, Rev. Mineral. Geochem. 74 (2012) 211-278. https://doi.org/10.2138/rmg.2012.74.6.
[47] M. Liu, S. Hong, Y. Wang, J. Zhang, D. Hou, B. Dong, Compositions and microstructures of hardened cement paste with carbonation curing and further water curing, Constr. Build. Mater. 267 (2021) 121724. https://doi.org/10.1016/j.conbuildmat.2020.121724.
[48] R. Guo, Q. Chen, H. Huang, X. Hu, T. Wang, Carbonation curing of industrial solid waste-based aerated concretes, Greenhouse Gases: Sci. Technol. 9 (4) (2019) https://doi.org/10.1002/ghg.1862.
[49] X. Pan, C. Shi, X. Hu, Z. Ou, Effects of CO_2 surface treatment on strength and permeability of one-day-aged cement mortar, Constr. Build. Mater. 154 (2017) 1087-1095. https://doi.org/10.1016/j.conbuildmat.2017.07.216.
[50] J. Li, W. Zhang, P.J.M. Monteiro, Synchrotron x-ray Raman scattering shows the changes of the Ca environment in C-S-H exposed to high pressure, Cem. Concr. Res. 132 (2020) 106066. https://doi.org/10.1016/j.cemconres.2020.106066.
[51] R.-S. Lin, Y. Han, X.-Y. Wang, Macro–meso–micro experimental studies of calcined clay limestone cement (LC3) paste subjected to elevated temperature,

Cem. Concr. Compos. 116 (2021) 103871. https://doi.org/10.1016/j.cemconcomp.2020.103871.
[52] B. Xu, B. Lothenbach, F. Winnefeld, Influence of wollastonite on hydration and properties of magnesium potassium phosphate cements, Cem. Concr. Res. 131 (2020) 106012. https://doi.org/10.1016/j.cemconres.2020.106012.
[53] R.I. Khan, W. Ashraf, Effects of ground wollastonite on cement hydration kinetics and strength development, Constr. Build. Mater. 218 (2019) 150-161. https://doi.org/10.1016/j.conbuildmat.2019.05.061.
[54] K. Traoré, T.S. Kabré, P. Blanchart, Gehlenite and anorthite crystallisation from kaolinite and calcite mix, Ceram. Intl. 29 (4) (2003) 377-383. https://doi.org/10.1016/S0272-8842(02)00148-7.
[55] R. Hay, K. Celik, Accelerated carbonation of reactive magnesium oxide cement (rmc)-based composite with supercritical carbon dioxide (scCO2), J. Clean. Prod. 248 (2020) 119282. https://doi.org/10.1016/j.jclepro.2019.119282.
[56] G. Ye, X. Liu, G. De Schutter, A.M. Poppe, L. Taerwe, Influence of limestone powder used as filler in SCC on hydration and microstructure of cement pastes, Cem. Concr. Compos. 29 (2) (2007) 94-102. https://doi.org/10.1016/j.cemconcomp.2006.09.003.
[57] M. Abdel Wahab, I. Abdel Latif, M. Kohail, A. Almasry, The use of wollastonite to enhance the mechanical properties of mortar mixes, Constr. Build. Mater. 152 (2017) 304-309. https://doi.org/10.1016/j.conbuildmat.2017.07.005.
[58] P. Kalla, A. Rana, Y.B. Chad, A. Misra, L. Csetenyi, Durability studies on concrete containing wollastonite, J. Clean. Prod. 87 (2015) 726-734. https://doi.org/10.1016/j.jclepro.2014.10.038.
[59] W.A. Gutteridge, J.A. Dalziel, Filler cement: The effect of the secondary component on the hydration of portland cement: Part I. A fine non-hydraulic filler, Cem. Concr. Res. 20 (5) (1990) 778-782. https://doi.org/10.1016/0008-8846(90)90011-L.
[60] Y. Briki, M. Zajac, M.B. Haha, K. Scrivener, Impact of limestone fineness on cement hydration at early age, Cem. Concr. Res. 147 (2021) 106515. https://doi.org/10.1016/j.cemconres.2021.106515.
[61] P. He, C. Shi, Z. Tu, C.S. Poon, J. Zhang, Effect of further water curing on compressive strength and microstructure of CO2-cured concrete, Cem. Concr. Compos. 72 (2016) 80-88. https://doi.org/10.1016/j.cemconcomp.2016.05.026.
[62] Z. Tian, H. Ye, Electrical resistivity of partially-saturated alkali-activated slag containing sodium nitrite admixture, Cem. Concr. Compos. 120 (2021) 104053. https://doi.org/10.1016/j.cemconcomp.2021.104053.
[63] W. Ashraf, J. Olek, Carbonation behavior of hydraulic and non-hydraulic calcium silicates: Potential of utilizing low-lime calcium silicates in cement-based materials, J. Mater. Sci. 51 (13) (2016) 6173-6191. https://doi.org/10.1007/s10853-016-9909-4.
[64] K. Kobayashi, K. Suzuki, Y. Uno, Carbonation of concrete structures and decomposition of C-S-H, Cem. Concr. Res. 24 (1) (1994) 55-61. https://doi.org/10.1016/0008-8846(94)90082-5.

[65] P.J.M. Monteiro, G. Geng, D. Marchon, J. Li, P. Alapati, K.E. Kurtis, M.J.A. Qomi, Advances in characterizing and understanding the microstructure of cementitious materials, Cem. Concr. Res. 124 (2019) 105806. https://doi.org/10.1016/j.cemconres.2019.105806.
[66] IPCC, Fourth assessment report (AR4), Working Group I, UNEP, New York, 2007.
[67] C. Andrade, M.Á. Sanjuán, Updating carbon storage capacity of Spanish cements, Sustainability 10 (12) (2018) 4806. https://www.mdpi.com/2071-1050/10/12/4806.
[68] L.C. Dreyer, A.L. Niemann, M.Z. Hauschild, Comparison of three different lcia methods: EDIP97, CML2001 and Eco-indicator 99, Int. J. Life Cycle Asses. 8 (4) (2003) 191-200. https://doi.org/10.1007/BF02978471.
[69] J.B. Guinée, E. Lindeijer, Handbook on life cycle assessment: Operational guide to the ISO standards, Dordrecht: Kluwer Academic Publishers; 2002.
[70] R. Lacy, M. Molina, M. Vaca, C. Serralde, G. Hernandez, G. Rios, E. Guzman, R. Hernandez, R. Perez, Life-cycle ghg assessment of carbon capture, use and geological storage (CCUS) for linked primary energy and electricity production, Int. J. Greenhouse Gas Ctrl. 42 (2015) 165-174. https://doi.org/10.1016/j.ijggc.2015.07.017.
[71] E. Batuecas, F. Liendo, T. Tommasi, S. Bensaid, F.A. Deorsola, D. Fino, Recycling CO_2 from flue gas for $CaCO_3$ nanoparticles production as cement filler: A life cycle assessment, J. CO2 Util. 45 (2021) 101446. https://doi.org/10.1016/j.jcou.2021.101446.
[72] S. Ruan, C. Unluer, Comparative life cycle assessment of reactive MgO and Portland cement production, J. Clean. Prod. 137 (2016) 258-273. https://doi.org/10.1016/j.jclepro.2016.07.071.
[73] D. Huntzinger, T. Eatmon, A life-cycle assessment of Portland cement manufacturing: Comparing the traditional process with alternative technologies, J. Clean. Prod. 17 (2009) 668-675. https://doi.org/10.1016/j.jclepro.2008.04.007.
[74] T. Stengel, P. Schießl, 22 - life cycle assessment (lca) of ultra high performance concrete (uhpc) structures, in: F. Pacheco-Torgal, L.F. Cabeza, J. Labrincha, A. de Magalhães (Eds.), Eco-efficient construction and building materials, Woodhead Publishing2014, pp. 528-564.
[75] I.T. Mercante, M.D. Bovea, V. Ibáñez-Forés, A.P. Arena, Life cycle assessment of construction and demolition waste management systems: A Spanish case study, Int. J. Life Cycle Asses. 17 (2) (2012) 232-241. https://doi.org/10.1007/s11367-011-0350-2.
[76] M.E. Boesch, S. Hellweg, Identifying improvement potentials in cement production with life cycle assessment, Environ. Sci. Technol. 44 (23) (2010) 9143-9149. https://doi.org/10.1021/es100771k.
[77] L. Caneda-Martínez, M. Monasterio, J. Moreno-Juez, S. Martínez-Ramírez, R. García, M. Frías, Behaviour and properties of eco-cement pastes elaborated with recycled concrete powder from construction and demolition wastes, Mater. 14 (5) (2021) 1299. https://www.mdpi.com/1996-1944/14/5/1299.

[78] S.-M. Jian, B. Wu, N. Hu, Environmental impacts of three waste concrete recycling strategies for prefabricated components through comparative life cycle assessment, J. Clean. Prod. 328 (2021) 129463. https://doi.org/10.1016/j.jclepro.2021.129463.
[79] W. Xing, V.W.Y. Tam, K.N. Le, J.L. Hao, J. Wang, Life cycle assessment of recycled aggregate concrete on its environmental impacts: A critical review, Constr. Build. Mater. 317 (2022) 125950. https://doi.org/10.1016/j.conbuildmat.2021.125950.
[80] R. Kurda, J.D. Silvestre, J. de Brito, Life cycle assessment of concrete made with high volume of recycled concrete aggregates and fly ash, Resour. Conserv. Recycl. 139 (2018) 407-417. https://doi.org/10.1016/j.resconrec.2018.07.004.
[81] S.H. Chu, Y.K. Kong, Mathematical model for strength of alkali-activated materials, J. Build. Eng. 44 (2021) 103189. https://doi.org/10.1016/j.jobe.2021.103189.
[82] T. Wang, D.-C. Xiao, C.-H. Huang, Y.-K. Hsieh, C.-S. Tan, C.-F. Wang, CO_2 uptake performance and life cycle assessment of cao-based sorbents prepared from waste oyster shells blended with pmma nanosphere scaffolds, J. Hazard. Mater. 270 (2014) 92-101. https://doi.org/10.1016/j.jhazmat.2014.01.026.
[83] L. Giordano, D. Roizard, E. Favre, Life cycle assessment of post-combustion CO_2 capture: A comparison between membrane separation and chemical absorption processes, Int. J. Greenhouse Gas Ctrl. 68 (2018) 146-163. https://doi.org/10.1016/j.ijggc.2017.11.008.
[84] P. Van den Heede, N. De Belie, Environmental impact and life cycle assessment (LCA) of traditional and 'green' concretes: Literature review and theoretical calculations, Cem. Concr. Compos. 34 (4) (2012) 431-442. https://doi.org/10.1016/j.cemconcomp.2012.01.004.
[85] G. Leonzio, D. Bogle, P.U. Foscolo, E. Zondervan, Optimization of CCUS supply chains in the UK: A strategic role for emissions reduction, Chem. Eng. Res. Des. 155 (2020) 211-228. https://doi.org/10.1016/j.cherd.2020.01.002.
[86] Q. Li, Z.A. Chen, J.T. Zhang, L.C. Liu, X.C. Li, L. Jia, Positioning and revision of CCUS technology development in china, Int. J. Greenhouse Gas Ctrl. 46 (2016) 282-293. https://doi.org/10.1016/j.ijggc.2015.02.024.
[87] A. Saito, K. Itaoka, M. Akai, Those who care about ccs—results from a Japanese survey on public understanding of CCS, Int. J. Greenhouse Gas Ctrl. 84 (2019) 121-130. https://doi.org/10.1016/j.ijggc.2019.02.014.
[88] J. Ma, Y. Yang, H. Wang, L. Li, Z. Wang, D. Li, How much CO_2 is stored and verified through CCS/CCUS in China?, Energy Procedia 154 (2018) 60-65. https://doi.org/10.1016/j.egypro.2018.11.011.

List of Figures

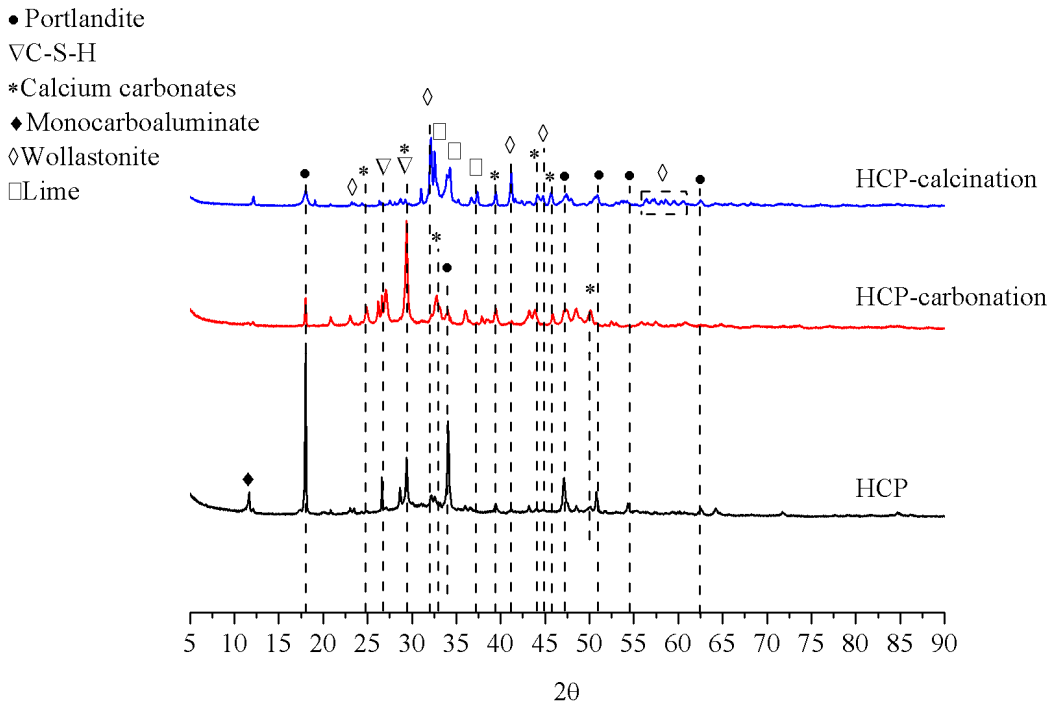

929

930 Fig. 1. XRD patterns of HCP, HCP-carbonation and HCP-calcination.

931

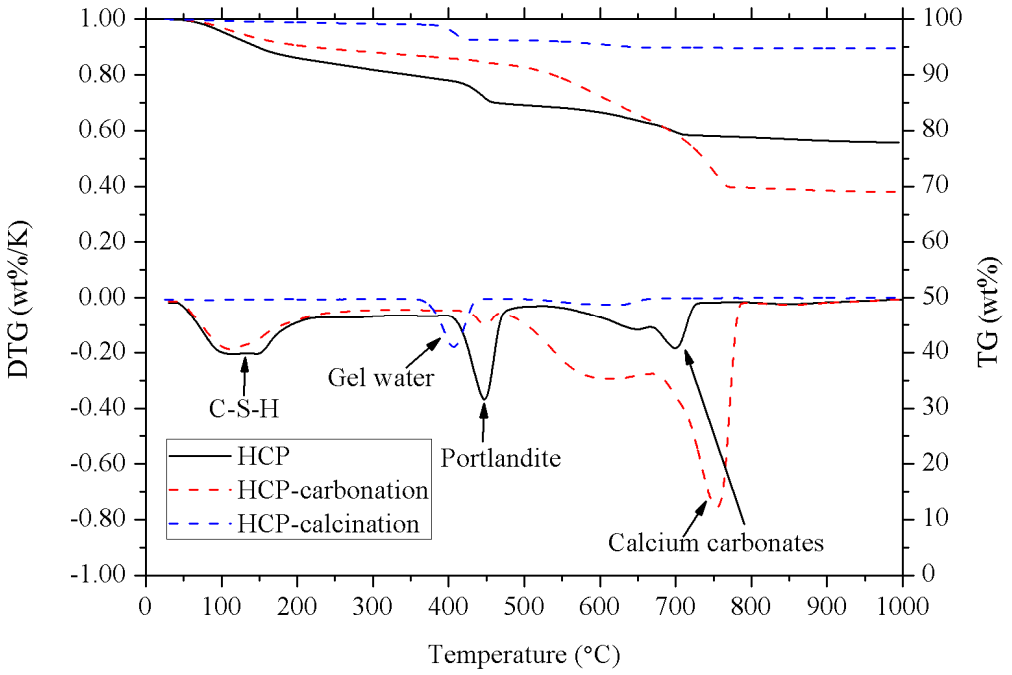

932

933 Fig. 2. TG and DTG curves of HCP, HCP-carbonation and HCP-calcination.

934

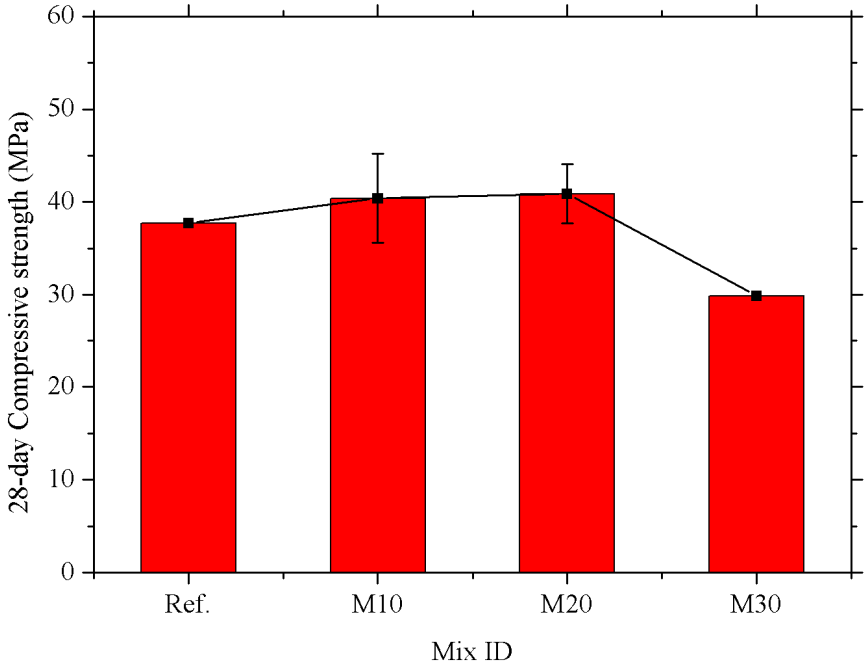

935

936 Fig. 3. Compressive strength results.

937

938

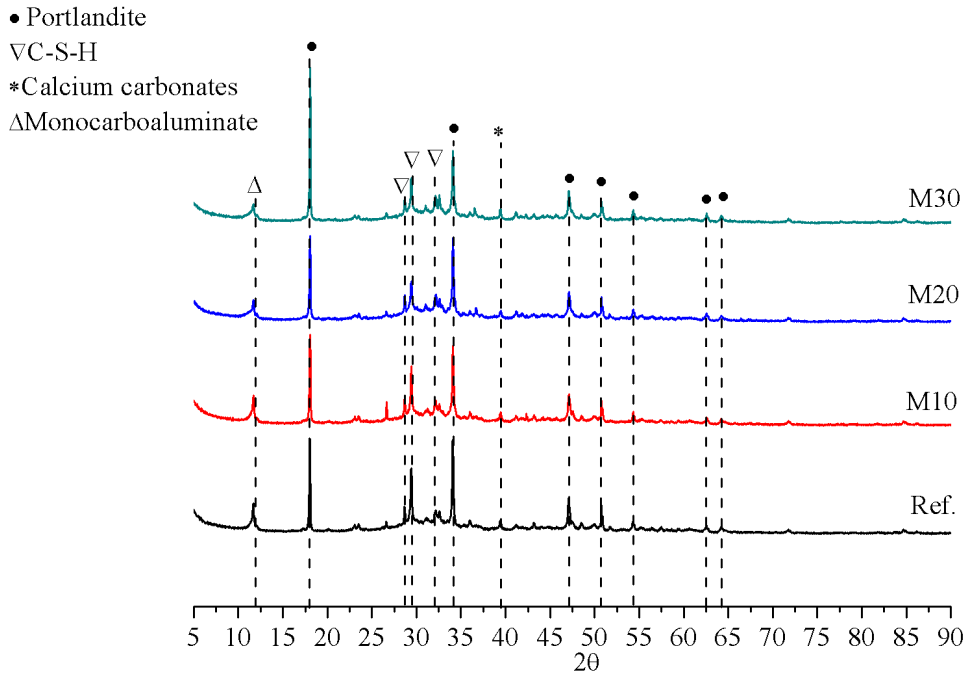

939

940 Fig. 4. XRD patterns of paste samples.

941

942

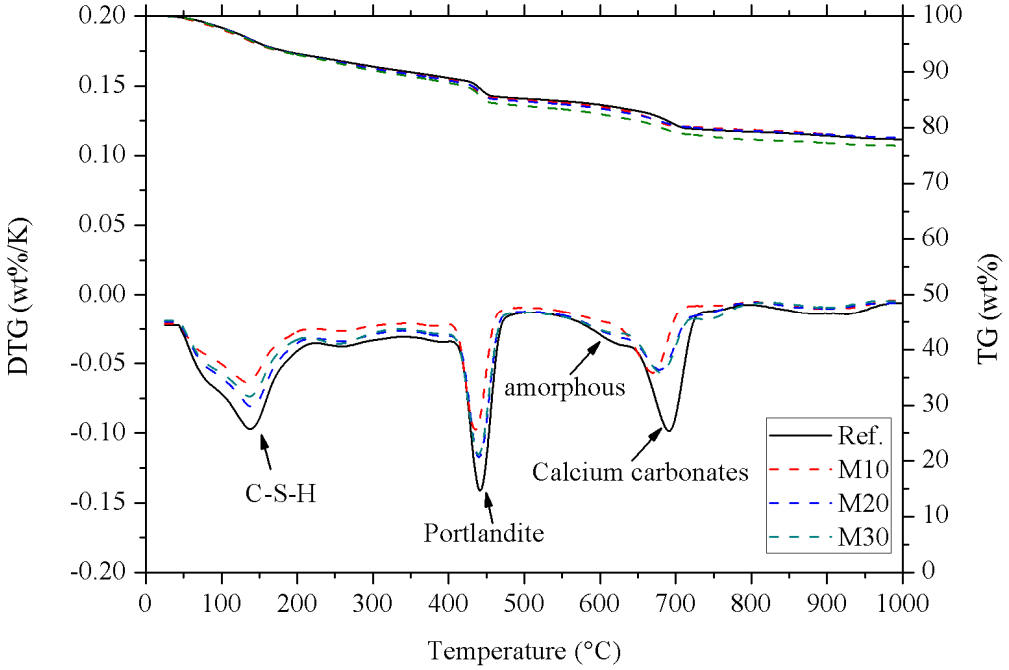

943

944 Fig. 5. TG and DTG curves of paste samples.

945

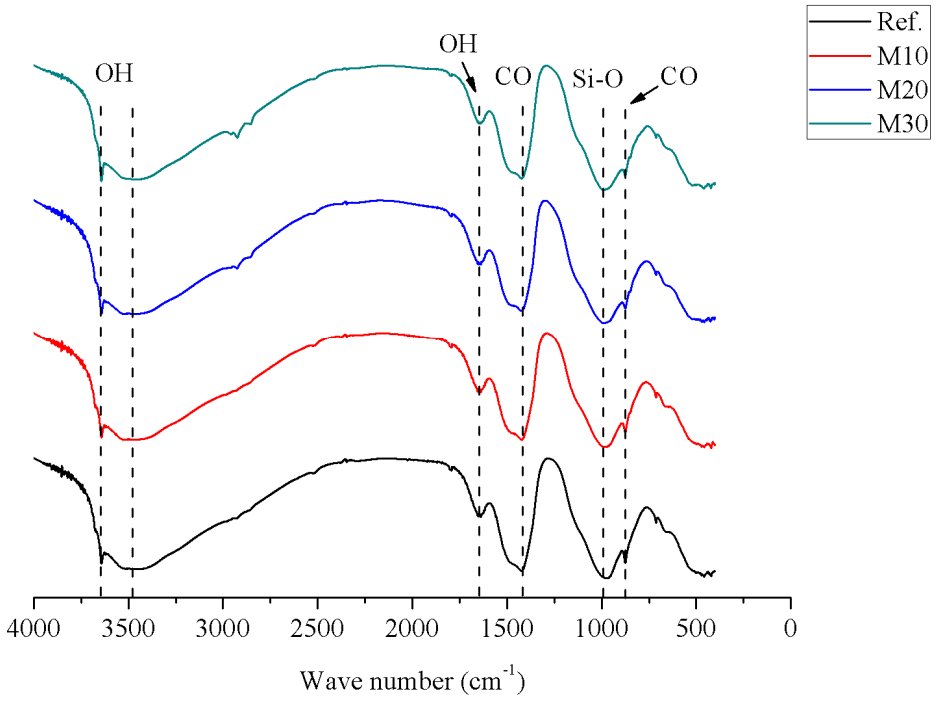

946

947 Fig. 6. FTIR spectra of paste samples.

948

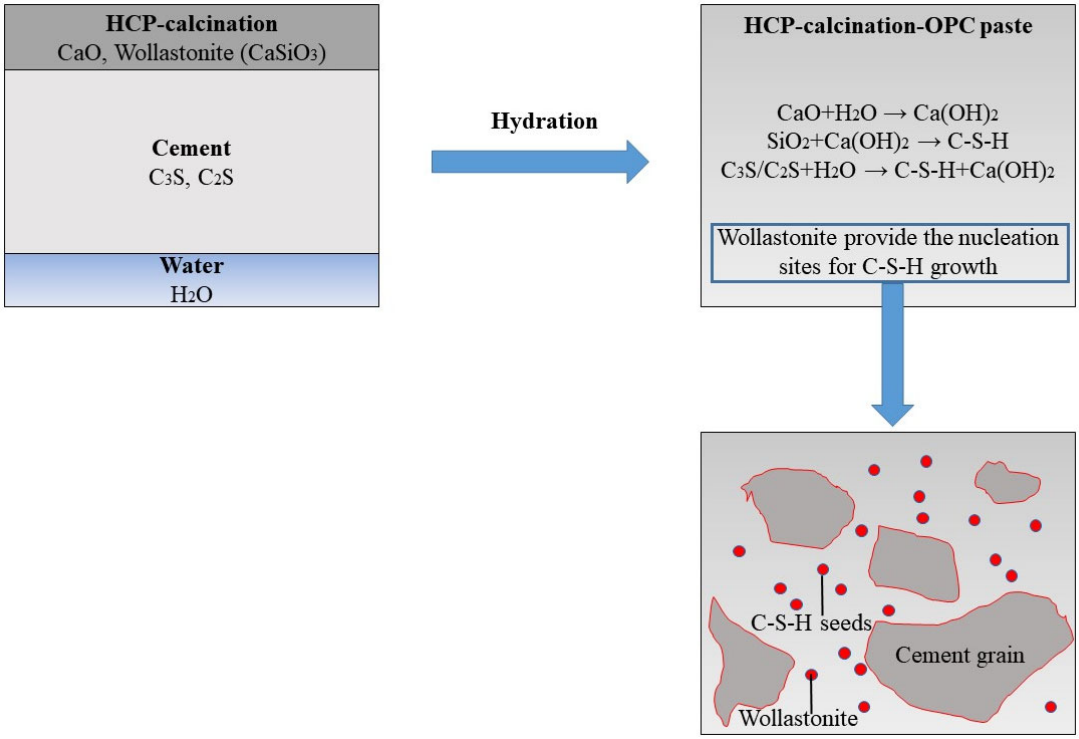

Fig. 7. Hydration behaviors of HCP-calcination-OPC pastes.

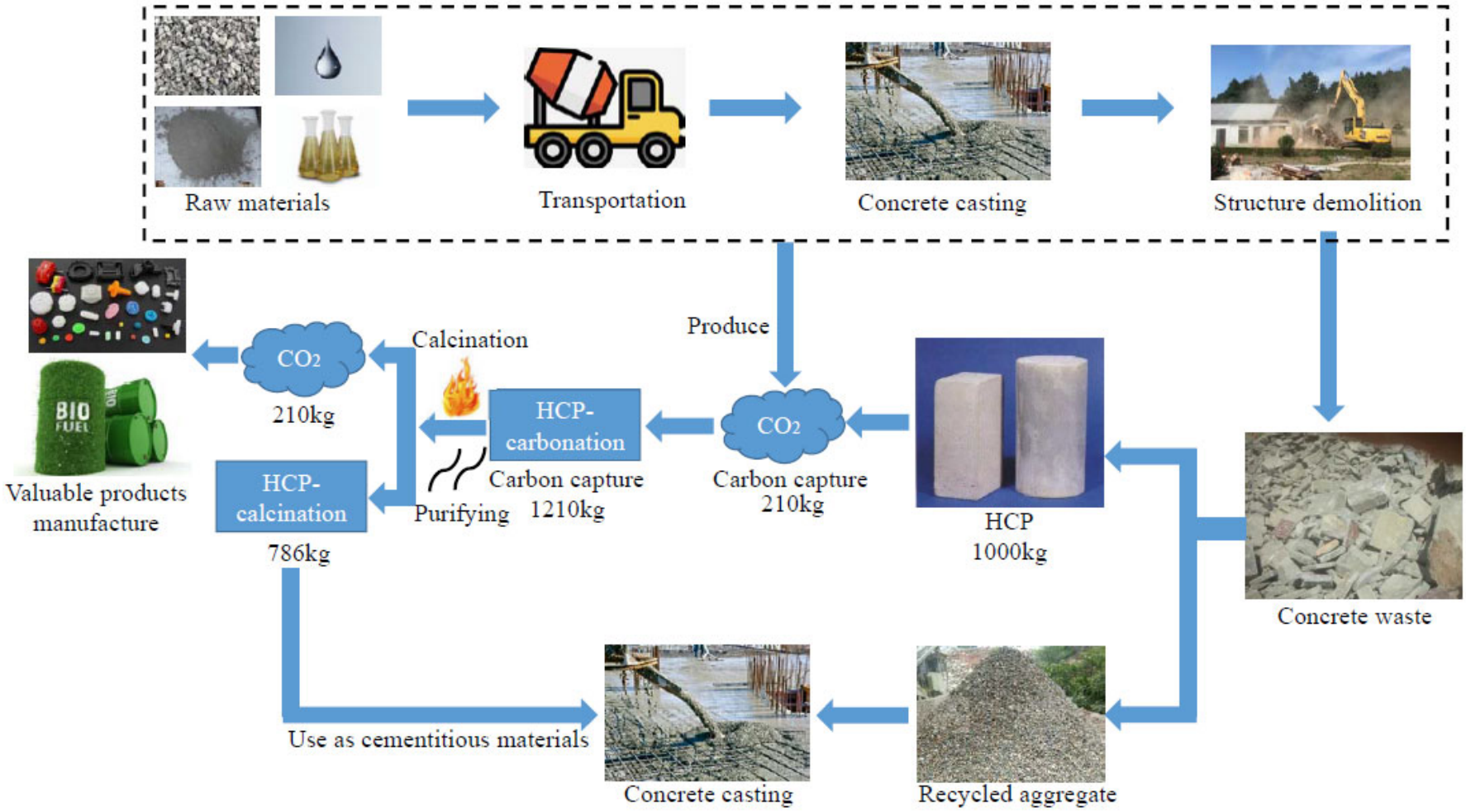

953

954 Fig. 8. Technology roadmap for CCUS using demolition waste

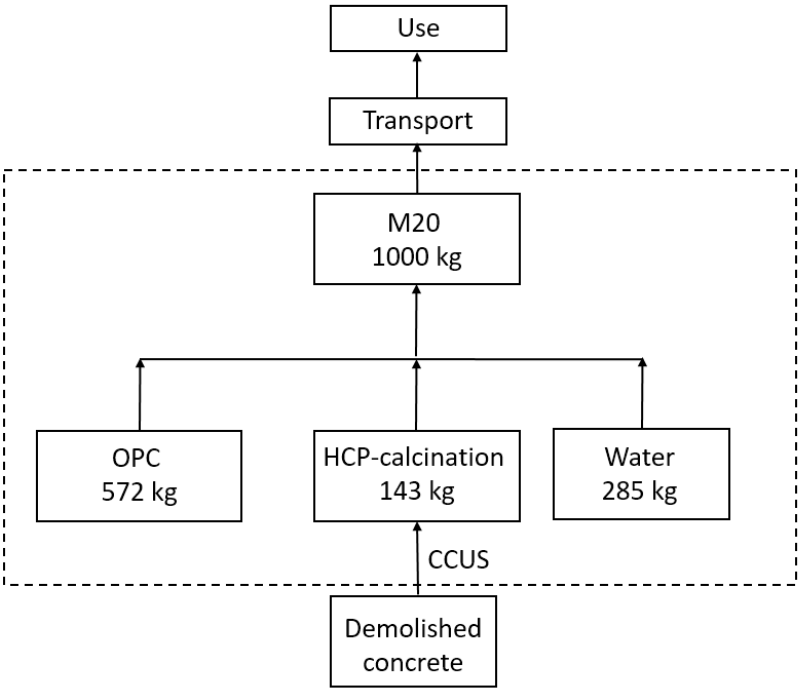

(a)

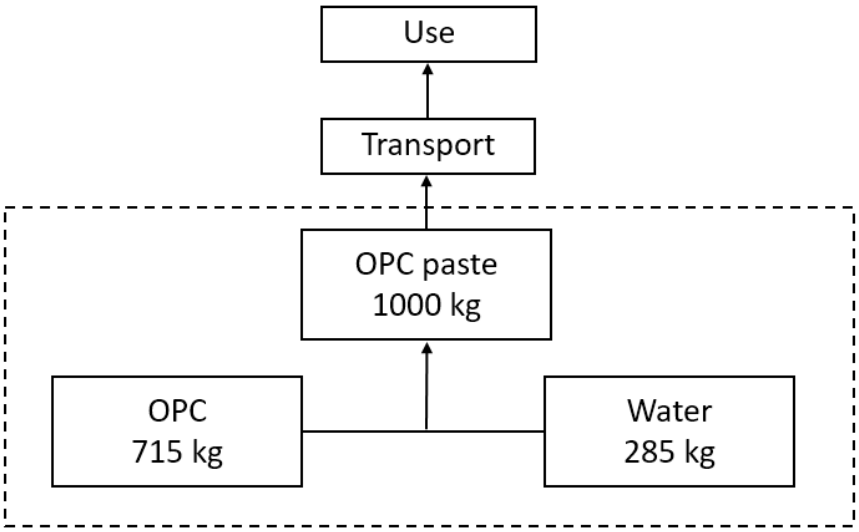

(b)

Fig. 9. The process and system boundaries of 1 tonne (a) M20 production and (b) OPC paste production.

962